INTERNATIONAL JOURNAL OF AUTOMOTIVE AND MECHANICAL ENGINEERING
ISSN: 2229-8649 e-ISSN: 2180-1606
VOLUME 22, ISSUE 4, 2025, 12920 - 12932
DOI: https://doi.org/10.15282/ijame.22.4.2025.6.0983

RESEARCH ARTICLE

Unsteady Drag Analysis of Platoon Vehicles using Unsteady Reynolds-Averaged Navier-Stokes and Improved Delayed Detached Eddy Simulation

Aan Yudianto*

Department of Mechanical and Automotive Engineering, Universitas Negeri Yogyakarta, Indonesia

ABSTRACT – The aerodynamic interaction of vehicles in platoon formation generates complex unsteady flow phenomena that strongly influence drag performance. This study investigates the unsteady aerodynamic drag and associated flow structures of two simplified Ahmed body models (30° slant angle) traveling in platoon using transient Computational Fluid Dynamics (CFD). Unsteady Reynolds-Averaged Navier–Stokes (URANS) and Improved Delayed Detached Eddy Simulation (IDDES) are employed to analyze the effect of longitudinal spacing ratios (*d/L*) ranging from 0.1 to 2.0. Following a mesh independence study, a grid with 13.3 million cells is adopted to resolve the flow field and quantify drag unsteadiness for both the lead and trailing vehicles across spacing configurations. Validation is performed by comparing the predicted drag coefficients with experimental measurements. Results show that the lead vehicle experiences a substantial drag reduction, with the coefficient decreasing to 0.16 at close spacing, before rising to 0.40 (URANS) and 0.37 (IDDES) at *d/L*=2. In contrast, the trailing vehicle exhibits only minor drag variation over *d/L* = 0.5–2, ranging from 0.35 to 0.37. Additional analyses include pressure coefficient distributions, instantaneous velocity fields, and vortex structures identified through Q-criterion visualizations. Comparisons indicate that IDDES captures finer flow structures and better reflects the unsteadiness of drag than URANS. Overall, the results suggest that the lead vehicle benefits most from platooning, achieving up to 60% drag reduction at small spacings, whereas the trailing vehicle gains comparatively little.

ARTICLE HISTORY
Received : 08th Dec. 2024
Revised : 15th June 2025
Accepted : 28th July 2025
Published : 16th Nov. 2025

KEYWORDS
Platoon
Drag
CFD
URANS
IDDES
Hybrid RANS-LES

1. INTRODUCTION

Vehicle platooning has emerged as a promising strategy to enhance fuel efficiency and reduce emissions in automotive transportation. The most common platooning configuration for road vehicles is observed in near-distance freight transport, where one or more truck platoons travel on highways and utilize drafting to achieve significant benefits. By allowing multiple vehicles to travel closely together, platooning reduces aerodynamic drag, thereby improving overall energy efficiency [1]-[4]. However, understanding the intricate fluid dynamics involved in vehicle platooning remains a significant challenge due to the complex and highly unsteady nature of flow interactions between vehicles, particularly under crosswind conditions[5]-[7]. The application of Unsteady Reynolds-Averaged Navier–Stokes (URANS) and Improved Delayed Detached Eddy Simulation (IDDES) in Computational Fluid Dynamics (CFD) enables detailed analysis of transient aerodynamic phenomena in vehicle platoons. URANS provides insight into overall aerodynamic forces and their temporal fluctuations with its ability to capture time-dependent variations in the mean flow field. In contrast, IDDES, a hybrid model combining the benefits of Reynolds-Averaged Navier–Stokes (RANS) and Large Eddy Simulation (LES), offers greater capability in resolving large-scale turbulent structures and vortices. This approach provides a more comprehensive understanding of unsteady aerodynamic interactions [8], [9], leading to more accurate predictions of drag coefficients and improved visualization of flow patterns[10], [11].

A study on vehicle platoon configurations has demonstrated a significant contribution to overall drag efficiency. For example, Altinsik et al. [12] investigated improvements in drag force for two realistic car models operating in a platoon configuration. A reduction in the lead vehicle's drag coefficient was observed in both experimental measurements and steady-state RANS CFD simulations. The rear vehicle, however, achieved aerodynamic improvement when the spacing distance equaled the vehicle length. In general, the lead vehicle benefits more than the rear vehicle in a platoon configuration. Similar results have also been reported by Yudianto et al.[13], Cerutti et al. [14], Paglianera et al. [15], and Watkins and Vino [16]. Conversely, when the platoon alignment is not perfectly in line, changes in drag performance affect the misaligned vehicle, reducing the benefits of the platooning formation [17], [18].

Due to the complex shape of realistic vehicle bodies and the need for validation studies, some researchers rely on simplified vehicle models. Luo et al. [19] employed the RANS CFD model to study platooning using the Ahmed body [20] and identified several longitudinal and lateral positions representative of vehicle overtaking. Complex aerodynamic behavior and variations in drag were observed in both the lead and rear vehicle models. Additionally, the number of vehicles in a platoon and the external shape of the vehicles also influence aerodynamic performance. Wang et al. [21] showed that different edge radii affect the drag coefficient, based on observations of simplified models representing

*CORRESPONDING AUTHOR | A. Yudianto | ✉ aan.yudianto@uny.ac.id

fastback, notchback, and squareback configurations. The calculations were performed computationally and included comparisons across different Reynolds numbers in the CFD simulations.

CFD simulations provide a powerful tool for capturing detailed flow characteristics. This study employs both URANS and IDDES methodologies to investigate the aerodynamic behavior of vehicle platoons. Specifically, the unsteadiness of the drag coefficient is measured, and comprehensive flow visualizations are provided to explain the turbulent structures and wake interactions that influence drag forces. The insights from this work aim to contribute to the optimization of platooning strategies to enhance vehicular performance and sustainability [22]. Despite advances in numerical methods in CFD and the growing number of studies on vehicle platoon efficiency, several areas remain underexplored. Existing research often focuses on steady-state analysis or simplified models that do not adequately capture the dynamic nature of the flow around closely spaced vehicles. This study addresses these gaps by employing both URANS and IDDES to conduct detailed simulations of vehicles in a platoon. The first objective is to measure drag unsteadiness, while the second is to visualize the complex wake flow behavior of two closely traveling vehicles. Ultimately, this study provides deeper insight into the transient aerodynamic behavior of platooning vehicles and contributes to the development of more efficient and optimized platooning strategies for road transport.

2. COMPUTATIONAL DOMAIN AND NUMERICAL FLOW CONDITIONS

The vehicle model is characterized by the Ahmed Body [20], which has been widely used by many researchers, including Watkins and Vino [16], who serve as the main reference for validating the results in this study. This work uses the 30° slant angle version, also referred to as the critical slant angle, where rapid changes in flow physics occur and strongly affect the vehicle's drag coefficient. The vehicle model's legs were included in this simulation. Details of the vehicle geometry are shown in Figure 1. The Reynolds number used in this study is based on the vehicle length (L) and the free-stream velocity U_∞ 35 m/s giving Re = 2.3x10^6, with flow in the +X direction as indicated in Figure 2. The chosen Reynolds number and vehicle spacing enable comparison with the reference data of Watkins and Vino [16].

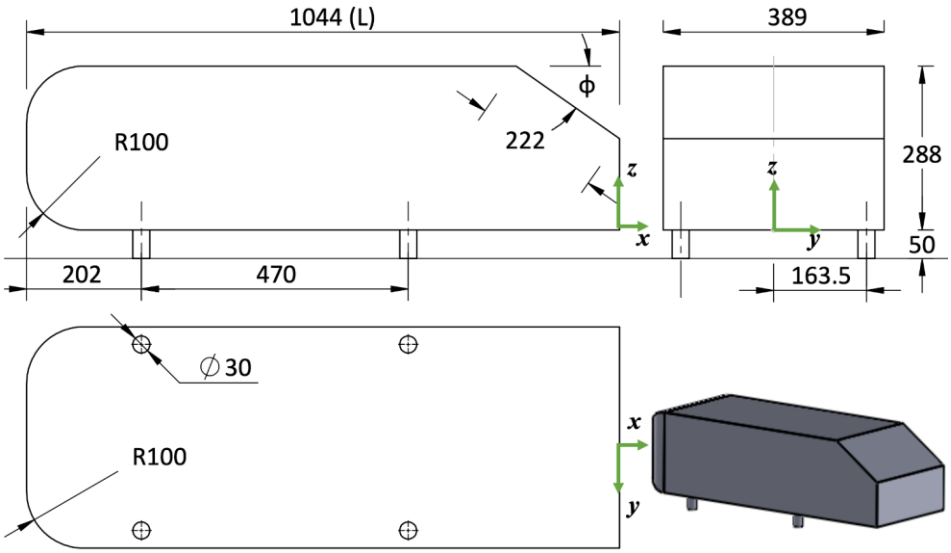

Figure 1. Ahmed's body [20] geometry for the isolated model

The computational domain used in this study is shown in Figure 2. Let *L* be the total vehicle length. The two vehicles in platoon configuration are placed in a virtual wind tunnel with a total length of *12L*, a total width of *3L*, and a total height of *1.5L*. The lead vehicle is positioned at a distance of *3L* from the computational inlet, and the spacing between vehicles is defined by the dimensionless parameter *d/L*, where *d* is the spacing distance. To eliminate boundary-layer effects at the lower boundary, the road surface was modeled as a slip wall, allowing tangential velocity without friction. The tunnel walls, including both sides and the upper boundary, were also set as slip walls to represent the far field. The outlet boundary was treated with a condition that switches between a fixed value when flow enters the domain through the outlet and a zero-gradient condition when flow exits, to account for possible flow reversal at this boundary.

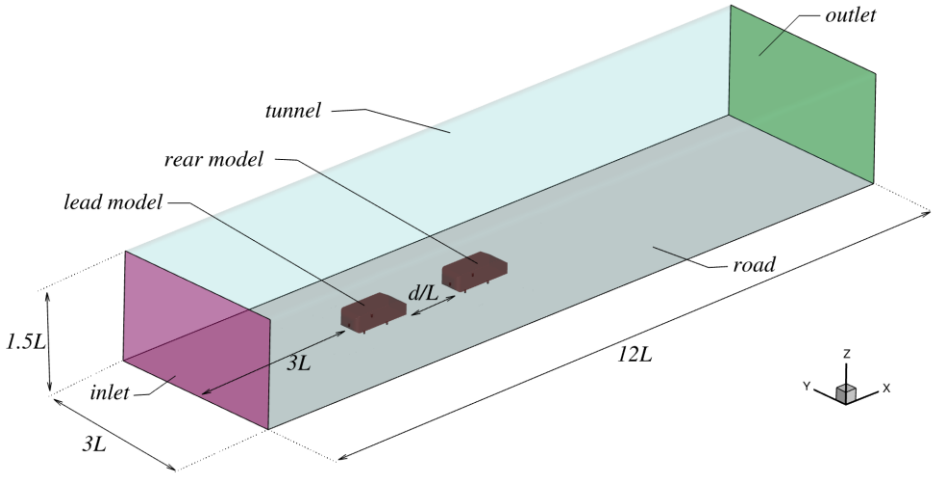

Figure 2. Computational domain

3. TURBULENCE MODELING

This numerical study of two vehicles travelling in platoon configuration uses both URANS and IDDES methods to solve the underlying turbulence model and evaluate the drag and associated fluid flow. The URANS method allows simulating turbulent flows that resolve the time-dependent, or unsteady, behavior of the main flow field. It accounts for time-dependent fluctuations in the flow, making the simulation more realistic of the real conditions of vehicle platooning. By using the Navier-Stokes equation with time dependency, it can capture the transient effects in the flow. The Reynolds averaging is made where the instantaneous quantities are decomposed into mean and fluctuating components. The turbulence modeling that is used is the one-equation Spalart-Allmaras (SA) turbulence model [23].

The SA turbulence model [23] is a widely used one-equation eddy-viscosity turbulence model for external aerodynamics. It solves a single transport equation for a modified turbulence kinematic viscosity, $\tilde{\nu}$. In the attached boundary layer and mildly separated flow, the model is proposed to provide a balance between accuracy and computational efficiency, which is suitable for vehicle aerodynamics. The transport equation, $\tilde{\nu}$, is given by

$$\frac{\partial \tilde{\nu}}{\partial t} + U_j \frac{\partial \tilde{\nu}}{\partial x_j} = C_{b1}(1 - f_{t2}) S \tilde{\nu} + \frac{1}{\sigma}[\nabla \cdot ((\nu + \tilde{\nu})\nabla \tilde{\nu}) + C_{b2} |\nabla \tilde{\nu}|^2] - \left[C_{w1} f_w - \left(\frac{C_{b1}}{\kappa^2} \right) f_{t2} \right] \left(\frac{\tilde{\nu}}{d} \right)^2 \quad (1)$$

where U_j is the velocity component of the flow, S is the vorticity magnitude, d is the distance from the wall, ν is the kinematic viscosity of the fluid. C_{b1},C_{b2},C_{w1},σ,κ are the model constants, and f_{t2}, f_w are empirical damping function. In this case, the eddy viscosity is calculated as:

$$\nu_t = \tilde{\nu} f_{v1} \quad (2)$$

where f_{v1} is another empirical function to ensure proper behavior near the wall. A more detailed explanation of this turbulence model can be seen in reference [23]. In this study, the SA model is employed to represent the Unsteady Reynolds-Averaged Navier–Stokes (URANS) simulations for assessing the behavior of the vehicle platoon under unsteady flow conditions.

Additionally, the work in this study also employs the IDDES, which can combine the features of RANS and LES, benefiting from the strengths of both simulation methods. Essentially, this hybrid approach uses the RANS model to solve the flow equation near the walls and in a region in which the turbulence scales are small and computationally expensive to resolve. Instead, the LES approach is used in the region far from the wall, where larger turbulence structures dominate, and it is sufficient to resolve them directly. Accuracy, efficiency, and flexibility can be achieved by using this method. Realizing that the flow predictions of complex flows can be accurately simulated, the need for a finer mesh in the near-wall region can be reduced, and both attached and separated flows can be handled. The Spalart-Allmaras IDDES from Gritskevich et al. [24] is utilized in this study. The governing equation for SA-IDDES remains the same as the original SA model in Equation (1). However, the distance from the wall is replaced by. The modified length scale d_{IDDES}, which determine the switching between RANS and LES region.

$$d_{IDDES} = d - f_d \cdot \max(0, d - C_{DES}\Delta) \quad (3)$$

where Δ is the grid length scale, which in this case is the local grid spacing, C_{DES} is a model constant, and f_d is a shielding function to prevent premature switching to LES in attached boundary layers. In the attached region, where $d_{IDDES} = d$, the model behaves as a standard SA-RANS model. However, in a separated region with a finer grid, the $d_{IDDES} \rightarrow C_{DES}\Delta$, which allows LES-like resolution of the large-scale turbulent structures. A more detailed formulation can be seen in reference [25]. This capability is especially suitable for resolving unsteady wakes and large-scale vortices arising from this particular case of vehicle platooning configuration.

4. TEMPORAL AND SPATIAL SETTINGS

It is widely known that the high computational cost of fully resolved LES is primarily due to the requirement for very fine mesh resolution in the boundary layer to accurately capture fluid flow in this region. The benefit of IDDES lies in overcoming this need by employing a RANS layer in the near-wall region, thereby relaxing the fine mesh requirement. In this work, a wall function is also used to model the near-wall region of turbulent flow, providing an efficient alternative by bridging the gap between the wall and the first computational grid point. This avoids the need for very fine mesh resolution near the walls. Accordingly, all calculations were carried out by maintaining the dimensionless wall distance y^+ between 30 and 300.

The transient simulations in this work were solved using the PISO (Pressure Implicit with Splitting of Operators) algorithm, which is an efficient method for solving the Navier–Stokes equations, especially in unsteady problems. The calculations were performed with the native OpenFOAM solver *pisoFoam*. Both URANS and IDDES were used to simulate the flow for a physical time of 3 seconds with a time step of $1x10^{-3}$. To ensure convergence of unsteady drag, the first 0.5 seconds of the simulation were excluded, and statistical averaging of the quantities of interest was performed over the remaining 2.5 seconds. Drag quantification averaging followed the convergence of unsteady drag, which will be explained in the next section. Recognizing that the smallest mesh elements are located in the near-wall region—generally solved with RANS and a wall function—the Courant–Friedrichs–Lewy (CFL) number for the fine mesh could be kept around one under this consideration.

5. MESH STUDY

The mesh study of the isolated vehicle is discussed in this section. Three different mesh sizes were chosen, and the corresponding drag coefficient (*Cd*) was calculated and compared for the isolated model. The coarse, medium, and fine meshes contained 0.4 million, 3 million, and 13.3 million cells, respectively. The y^+ values along the vehicle surface are approximately 50. This wall resolution is considered appropriate because the turbulence models used in this study, Spalart–Allmaras URANS and SA-based IDDES, are designed to operate with wall functions in the logarithmic region of the boundary layer, where y^+ values between 30 and 300 are typically recommended. Maintaining $y^+ \approx 50$ ensures that the boundary layer near the wall is adequately captured using standard wall function approaches without requiring excessive grid refinement.

Figure 3 compares the drag coefficient *Cd* for the three mesh sizes using both URANS and IDDES. It also shows the drag unsteadiness of the three meshes with different turbulence models over the simulation time. For URANS, the drag convergence of the coarse mesh appears to be achieved faster than the other two. The coarse mesh begins to converge after about 0.2 seconds, while the medium and fine meshes require more time to stabilize, reaching convergence at approximately 1.5 and 1.1 seconds, respectively. In contrast, both the coarse and fine meshes solved with IDDES show faster drag convergence, with values stabilizing before 0.5 seconds and remaining steady throughout the simulation. The medium mesh, however, appears to still be in the process of converging over the simulation time.

The comparison of unsteady drag coefficients shows that URANS produces less fluctuation in drag compared to IDDES. Since IDDES resolves more detailed turbulent structures, including unsteady wake dynamics, it provides a more physically realistic prediction of the drag coefficient. URANS, relying on turbulence modeling, tends to smooth out such effects. Therefore, the physical behavior of the drag coefficient is better captured using IDDES rather than URANS.

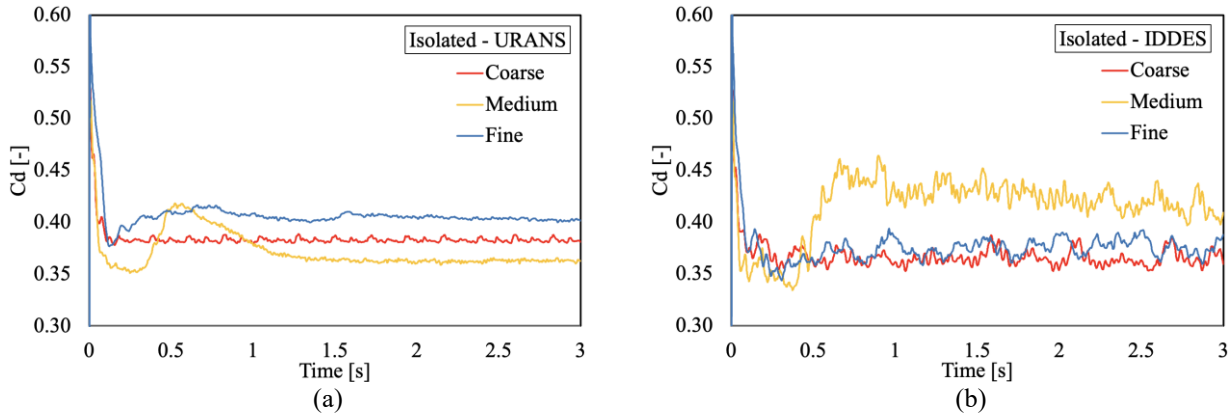

Figure 3. *Cd* different mesh of the isolated model calculated with (a) URANS and (b) IDDES

Using the same fine mesh settings as the isolated model, the mesh for the computational domain with different vehicle spacing distances was generated. The mesh comprises two levels of refinement regions: one close to the body to capture detailed turbulence structures and another further away, as shown in Figure 4. The figure illustrates only the fine mesh; however, the coarse and medium meshes use similar settings, with differences only in element size, resulting in different total cell counts. Inflation layers were also generated in the near-wall region along the body surface. The simulations were

performed in the fully scaled computational domain, while half-domain visualizations were used to better illustrate the location of the refinement regions.

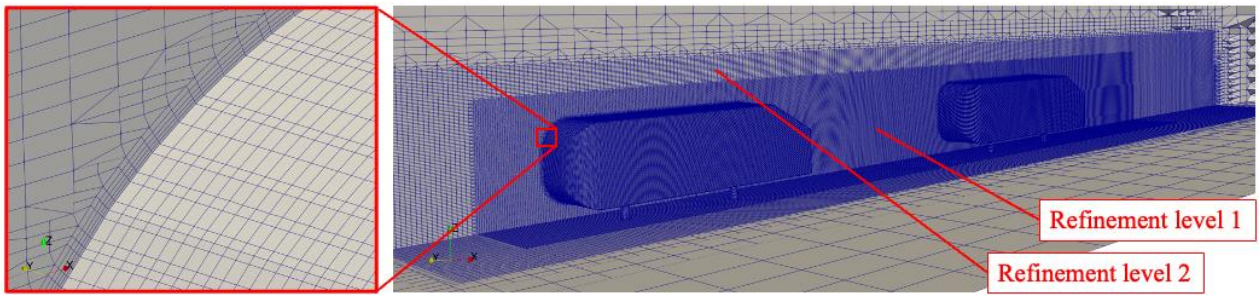

Figure 4. The fine mesh shows the two different refinement levels and the inflation layers close to the body

The results of the isolated model are validated by comparing this work with the original calculation by Ahmed et al. [20] and the study by Kohri et al. [26]. Similar work was also conducted by Guilmineau [27]. Both researchers reported that the 30° slant angle of the Ahmed body leads to substantially different drag results. When the slant angle is smaller than this critical value, the wake flow exhibits a highly three-dimensional structure, commonly referred to as dimensional separated flow. Conversely, when the slant angle exceeds this critical value, the flow structure becomes more two-dimensional, known as quasi-axisymmetric separated flow. This explains the differences in the resulting drag shown in Figure 5.

When the drag coefficient *Cd* results of the coarse, medium, and fine meshes are compared and averaged after 1.5 seconds, the values obtained in this study are comparable to previous works, although some discrepancies exist due to the critical angle condition, which has also been noted in earlier studies. Based on the results of the mesh independence study, all computational results presented in the results section are calculated using the fine mesh with 13.3 million cells.

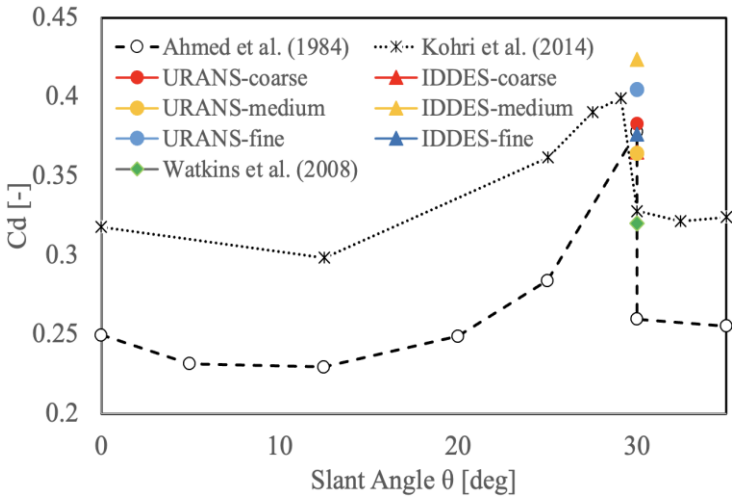

Figure 5. *Cd* after statistical averaging from 1 second onwards and the comparison to the previous works with different slant angles

6. RESULTS AND DISCUSSION

This section presents the results of drag unsteadiness, validation of the drag coefficients for both the lead and rear vehicles, discussion of similar findings from previous works, and flow field analysis in terms of pressure coefficient contours, instantaneous velocity, and flow visualization using the Q-criterion, obtained with two different turbulence models: URANS and IDDES.

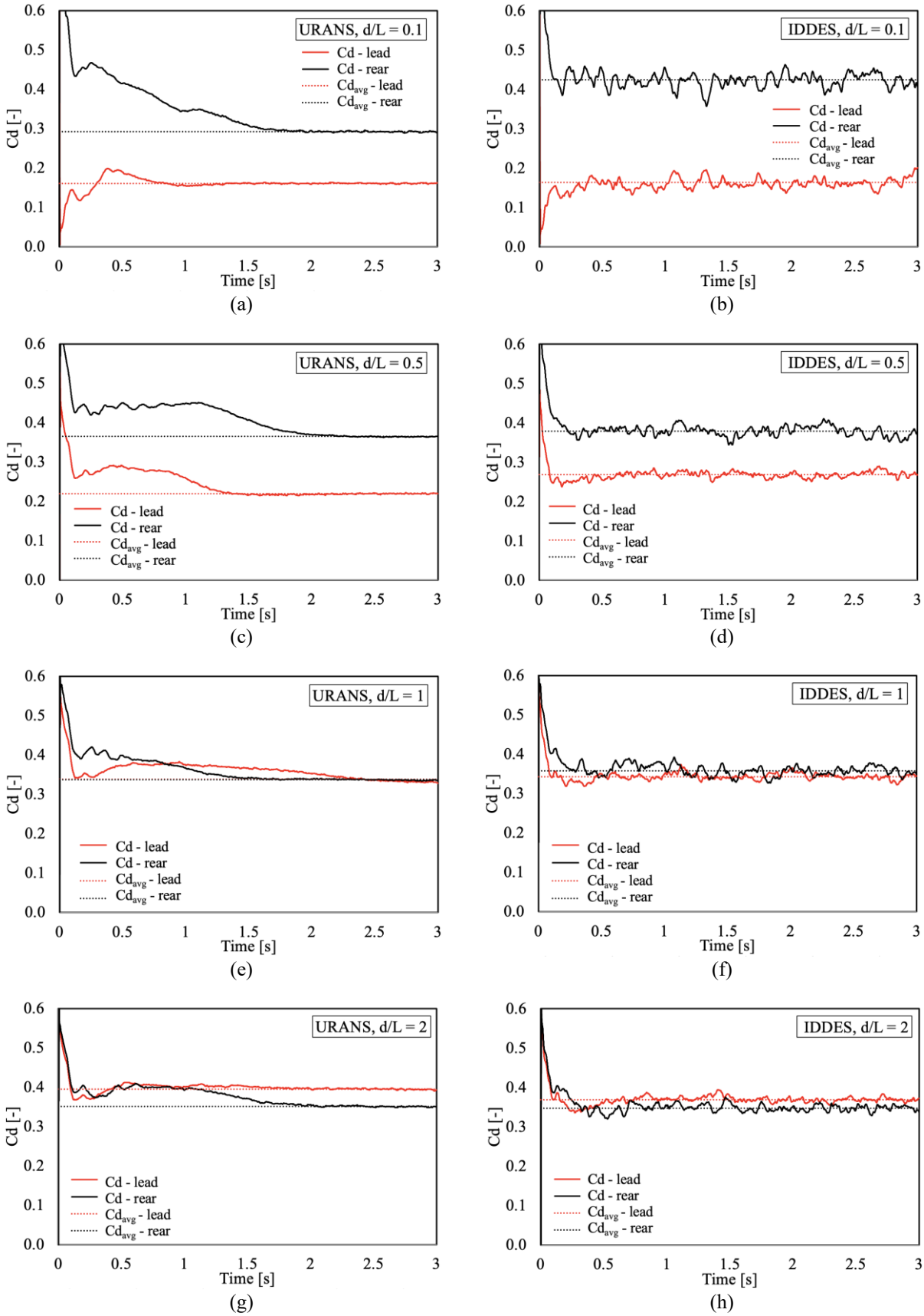

Figure 6. Unsteady drag convergence during the simulation time for both lead and rear models (a) and (b) at *d/L*=0.1, (c) and (d) at *d/L*= 0.5, (e) and (f) at *d/L*= 1, (g) and (h) at *d/L*= 2

Figure 6 compares the unsteady drag recorded during the simulation time for both the lead and rear vehicles using either the URANS or IDDES method. Each subfigure represents a different spacing distance *d/L* for each platooning configuration. Overall, the unsteady RANS simulation results in relatively more stable changes of the drag coefficient over the simulation time, while the IDDES results fluctuate within a threshold value of the drag coefficient because it also

resolves the large eddies occurring in the flow domain. With the current temporal and spatial settings of the simulation, the drag coefficient measured with the URANS method requires some time to reach a steady state, which is achieved after approximately 1.5 seconds of simulation time. In contrast, the IDDES solution reaches steady-state drag convergence much faster, with values stabilizing in less than the first 0.5 seconds of the simulation in most cases.

A clear effect of the inter-vehicle distance can also be observed on the unsteady drag of each vehicle. A significant difference in drag is found when d/L equals 0.1 and 0.5. However, at larger spacing distances of d/L = 1 and 2, the drag coefficients of both the lead and rear vehicle models show closer and more similar values. These results are consistent with the studies conducted by Ebrahim and Dominy [28] and by Schito and Braghin [29], which reported considerable drag reduction when vehicle spacing was d/L = 0.5 or lower, even with different vehicle geometries. In this study, the comparison of average drag coefficients was made after the drag reached a steady-state value, which occurs after 1.5 seconds for URANS. Accordingly, the average Cd indicated by the dotted line in all the graphs (URANS and IDDES) in Figure 6 represents the average value after 1.5 seconds. Smaller inter-vehicle distances strongly influence the drag of both vehicles, while larger spacings of d/L = 1 or 2 result in less pronounced effects. The aerodynamic benefits of drag reduction are more significant for the lead vehicle at close spacing, whereas the rear vehicle experiences fewer advantages in terms of drag coefficient reduction.

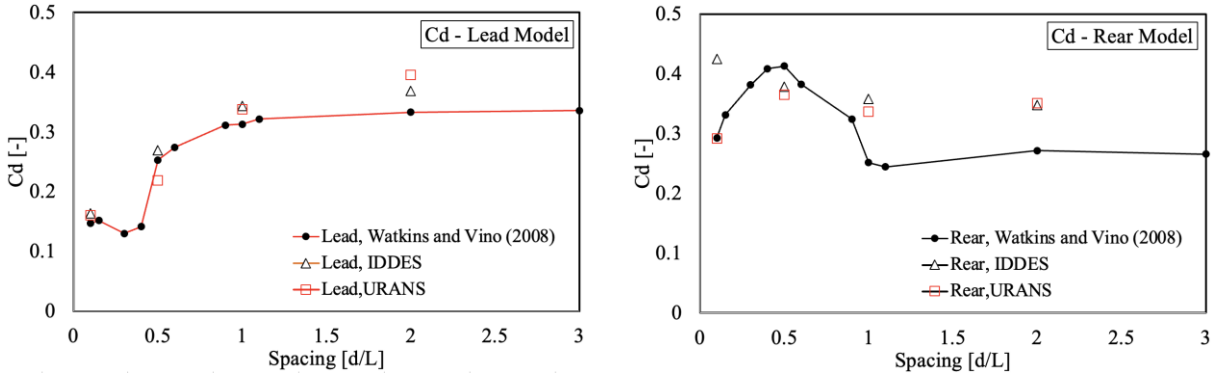

Figure 7. Drag coefficient at different inter-vehicle spacing of (a) Lead Model and (b) Rear Model compared to experiment by Watkins and Vino (2008)

The results of Cd are validated by comparison with the experimental measurements of Watkins and Vino [16], and Figure 7 shows the current drag calculations with both URANS and IDDES compared to the experimental results. In this case, the average drag after 1.5 seconds is used. The Cd of the lead vehicle model generally agrees with the experiments for the investigated d/L distances. Although some discrepancies are observed at d/L = 2 for both IDDES and URANS, the overall trend of the lead vehicle model agrees with the experimental results. Since the case of two vehicles travelling is challenging, the flow over the lead model influences the downstream flow conditions and affects the aerodynamic performance of the rear vehicle. The current results show some discrepancies in the Cd of the rear model compared with the experimental data. These differences may be attributed to the calculation settings, solver fidelity, and the need for a more refined mesh. However, considering the nature of the fluid flow, these discrepancies can be regarded as under-relaxation and addressed in future studies.

To further discuss the current results of drag reduction obtained by vehicles travelling in platoons, comparisons are made with results from other researchers. Romberg et al. [30] measured the drag of a race car during the passing process using wind tunnel experiments. Zabat et al. [31] reported the aerodynamic performance of vehicle platooning using a scaled prototype model. Pagliarella et al. [15] used a common vehicle reference model to assess platooning configurations, focusing on the relationship between vehicle geometry and aerodynamic performance during formation. Watkins and Vino [16] evaluated the effects of vehicle spacing on drag using a 30° slant angle Ahmed body in wind tunnel experiments. Cerutti et al. [14] measured the drag reduction of light commercial vehicles through wind tunnel experiments to assess the overall drag reduction of a group of vehicles travelling in a platoon. These previous works investigated similar aerodynamic performance using different measurement techniques, and a comparison with the present work is therefore made.

Figures 8 and 9 compare the normalized drag coefficient values experienced by the lead and rear vehicle models. Here, Cd represents the drag coefficient in platoon configuration, normalized by Cd_0, which is the drag coefficient of the isolated vehicle for each test case. Most studies indicate that the lead vehicle experiences greater drag reduction, improving its aerodynamic performance compared to the rear vehicle. A significant drag reduction is observed in most cases. The Cd of the lead vehicle increases with larger inter-vehicle distances (d/L), approaching the isolated model value when d/L = 2. Similar results have been reported in previous studies and are consistent with the present URANS and IDDES calculations. The behavior of the rear vehicle differs. Previous reports show that drag reduction is not always achieved for the rear vehicle as a function of inter-vehicle distance. Figure 9 shows that almost all studies report convergence to different normalized drag values for the rear vehicle. This indicates that drag variation in the rear vehicle

is strongly influenced by the lead vehicle flow conditions and the nature of the wake flow generated downstream. However, a similar trend of normalized *Cd* can be observed once $d/L \geq 1$, where no significant changes in *Cd* occur, which agrees with previous findings.

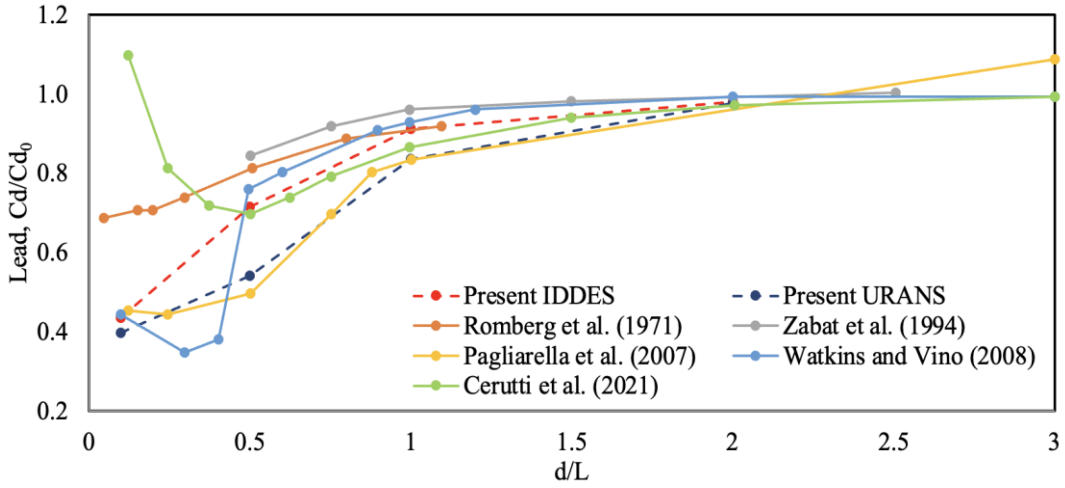

Figure 8. Normalized *Cd* in platoon compared to other references of the lead vehicle

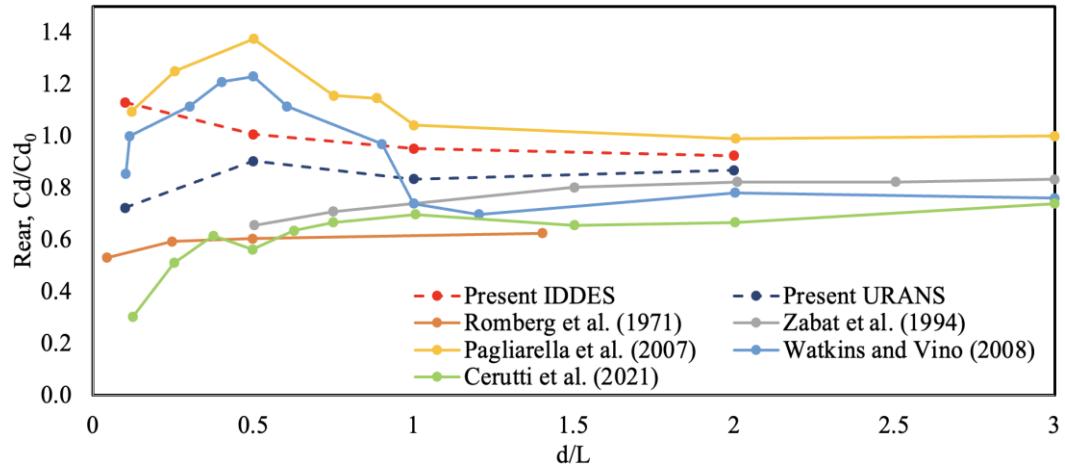

Figure 9. Normalized *Cd* in platoon compared to other references of the rear vehicle

Furthermore, Figures 10 and 11 present flow field analyses of the current study in terms of the pressure coefficient *Cp* at the mid-span plane of the computational domain. Figure 10 shows results from URANS, while Figure 11 shows results from IDDES. In both cases, pressure due to the stagnation point of the flow occurs at the front of the lead vehicle across all configurations. However, URANS shows a pronounced stagnation pressure at the front of the rear vehicle for $d/L = 1$ and 2. In contrast, IDDES predicts relatively high stagnation point pressure on the rear vehicle already at $d/L =$ 0.5, 1, and 2. This difference significantly affects the resulting drag, as discussed previously.

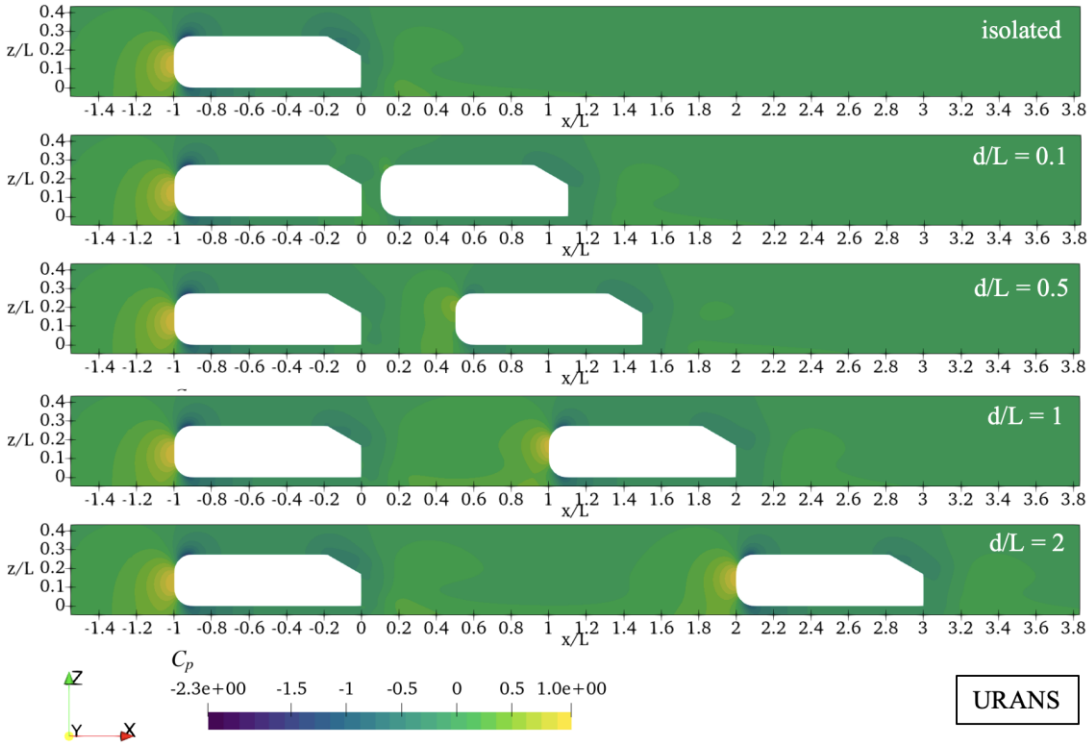

Figure 10. Pressure coefficient *Cp* calculated by URANS

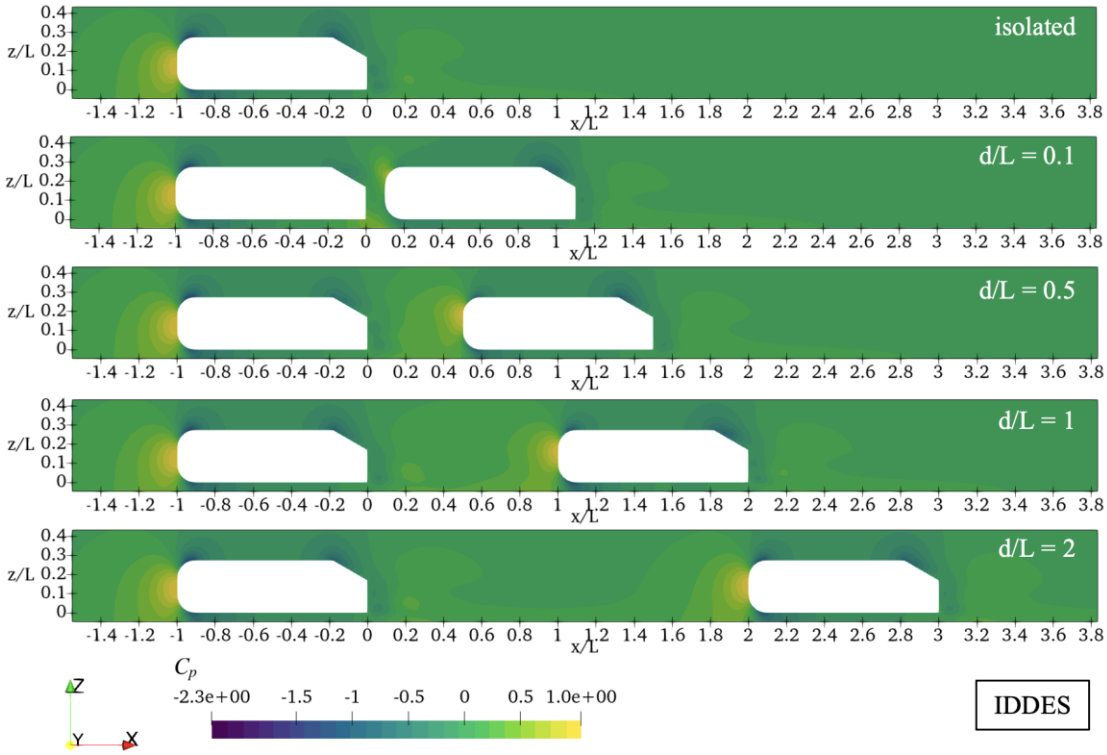

Figure 11. Pressure coefficient *Cp* calculated by IDDES

The effects of the flow field in terms of the instantaneous velocity contour at the symmetry plane provide further explanation of how the flow influences the drag coefficient of the vehicle model. Figures 12 and 13 compare the normalized instantaneous velocity, where U is the local velocity magnitude and U_∞ is the free-stream velocity. The URANS calculations predict low velocity in the region between the vehicles. This indicates that the flow behavior of the rear model is strongly influenced by the lead model at $d/L = 0.1$ and 0.5. However, the base wake of the lead vehicle does not appear to have a major effect on the rear vehicle when the spacing is $d/L = 1$ or 2. This corresponds to the drag of the rear vehicle beginning to stabilize at these distances.

The IDDES simulations, which can resolve large-scale turbulence in the computational domain, show slightly different results. Figure 13 compares the normalized velocity magnitude obtained with IDDES. With this method, the

wake in the rear part of the mid-plane can be visualized. At $d/L = 0.5$, the wake of the lead vehicle is directed downward and has less influence compared to the URANS results.

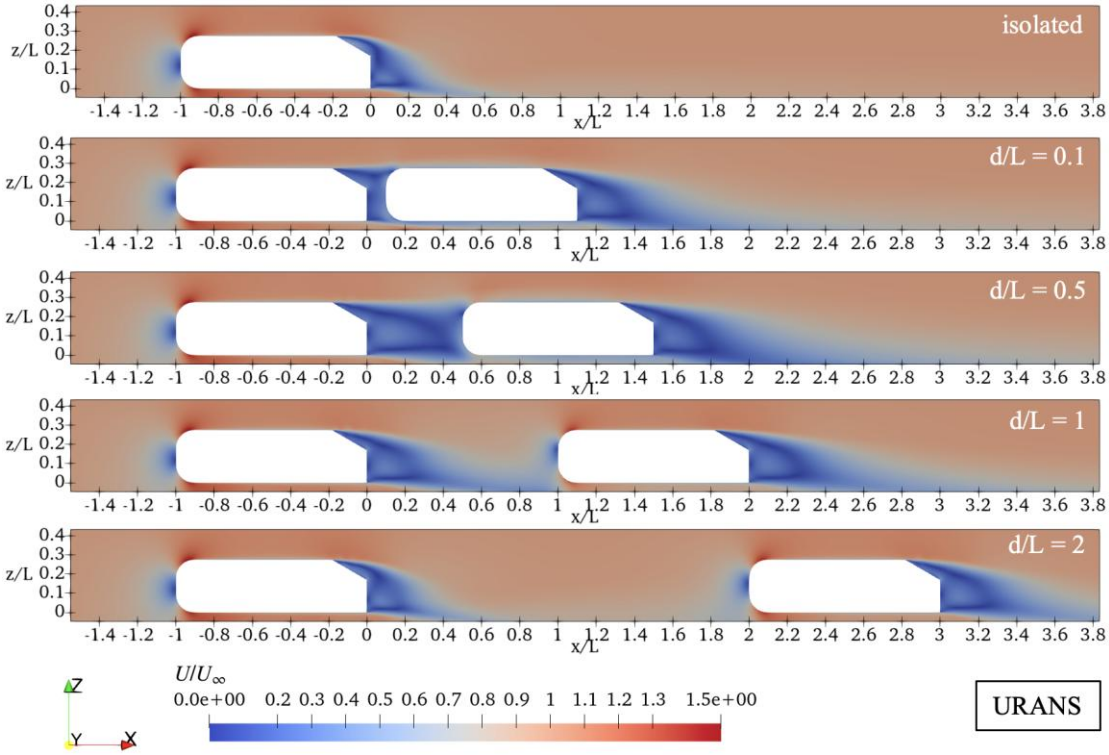

Figure 12. Normalized velocity U/U_∞ contour at mid-span plane calculated by using URANS at the latest timestep

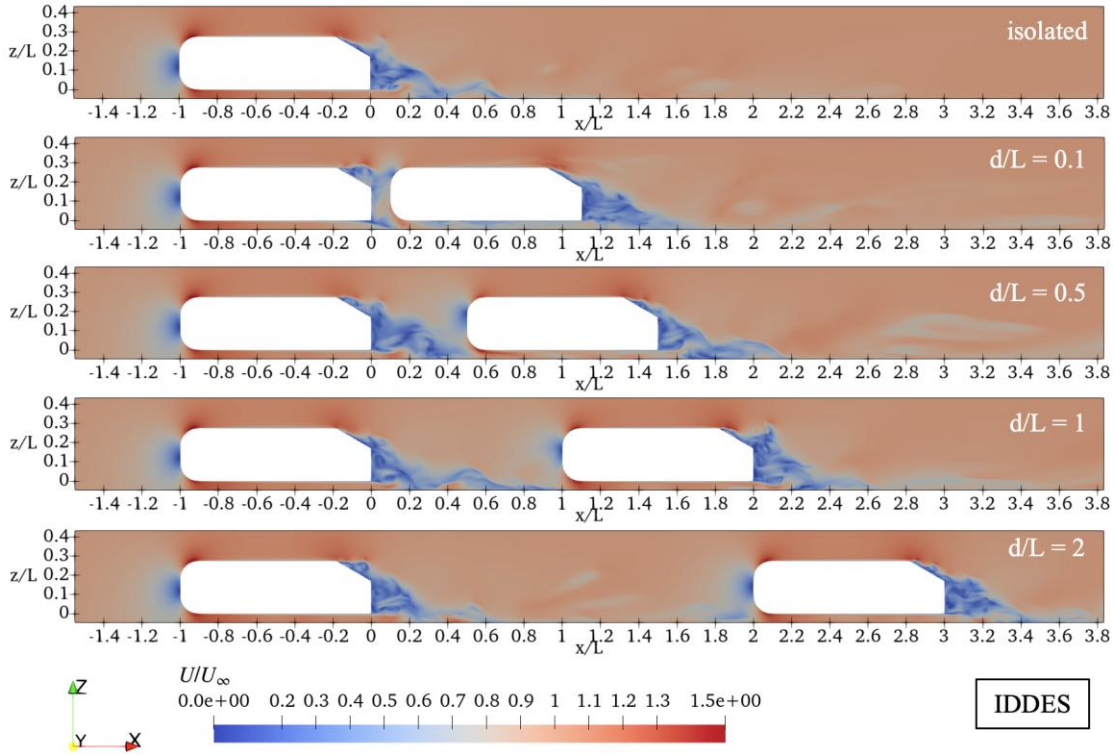

Figure 13. Normalized velocity U/U_∞ contour at mid-span plane calculated by using IDDES at the latest timestep

The three-dimensional flow around the vehicle can be visualized using the Q-criterion, defined as

$$Q = \frac{1}{2}(\| \Omega \|^2 - \| S \|^2) \tag{4}$$

where S is the strain rate tensor and Ω is the vorticity tensor. When $\Omega > 0$, local rotation dominates over strain, indicating the presence of a vortex core. Figures 14 and 15 compare the iso-surfaces based on a Q-criterion value of 1×10^5 for both

URANS and IDDES, for the isolated vehicle and for cases with spacing between vehicles. For URANS, the isolated vehicle shows a strong C-pillar vortex circulating inward after leaving the base. A lower vortex generated near the front part of the vehicle body is also observed. The backlight separation bubble, caused by the intersection between the roof and the rear slant angle, is also visible. However, when another vehicle is positioned directly behind the lead vehicle at a short spacing (d/L = 0.1), the flow behavior differs significantly from the isolated case. The C-pillar vortex and the backlight separation bubble are not generated due to the flow obstruction caused by the rear vehicle. As the spacing distance increases, the flow field develops, and at d/L = 2, the lead vehicle flow resembles that of the isolated model, with the C-pillar vortex reappearing. This, however, is not the case for the rear vehicle.

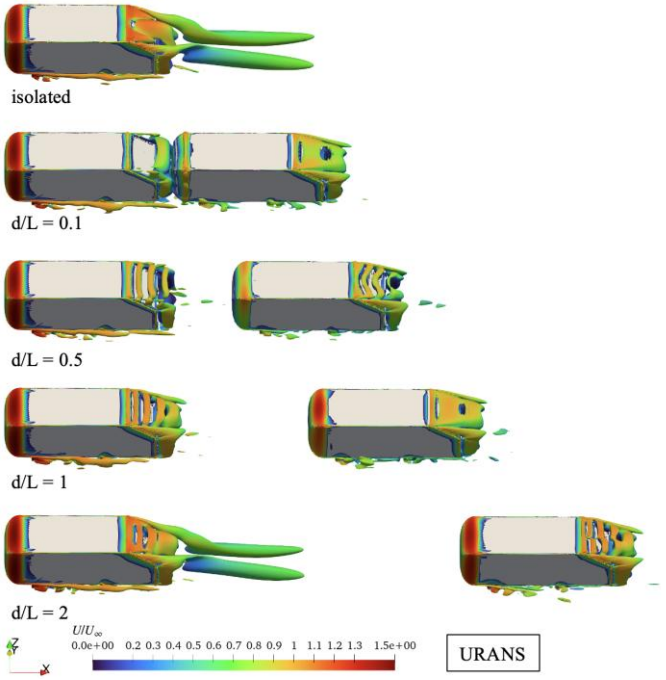

Figure 14. Q-criterion with the value of 1x10^5 and colored by normalized velocity U/U_∞ calculated by URANS

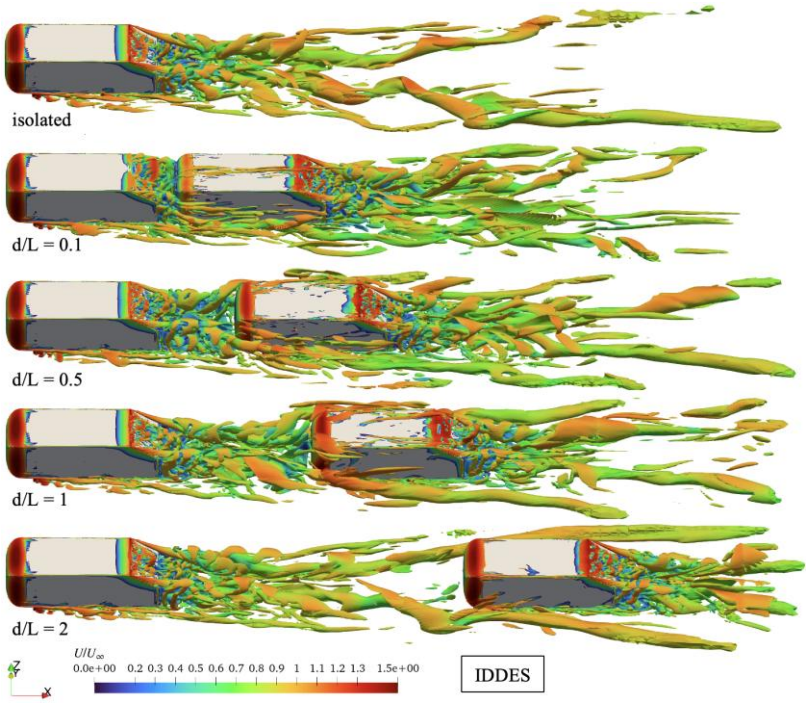

Figure 15. Q-criterion with the value of 1x10^5 and colored by normalized velocity U/U_∞ calculated by IDDES

The IDDES results are able to simulate and calculate in more detail the vortices generated by the vehicle, since this method resolves the large-scale turbulence occurring in the computational domain. The comparison of Q-criterion results is shown in Figure 15, with the color representing the normalized velocity magnitude. For the isolated vehicle, the C-pillar vortex is generated much further downstream from the vehicle model, and a more complex flow phenomenon can

be observed in this visualization. The lower part of the vehicle also generates a relatively complex flow field due to the presence of the vehicle legs. In this region, most of the flow is calculated using LES, as it is away from the wall where large eddies are present. The wake of the lead vehicle is influenced by the presence of the rear model when the spacing distance is short (d/L = 0.1). As also predicted by URANS, when d/L = 2, the wake develops similarly to that of the isolated model, and the C-pillar vortex of the rear model can also be observed. This uncertainty in vortex formation caused by the geometry contributes to the unsteadiness of the drag coefficient, as reported in the previous paragraph.

7. CONCLUSIONS

In this study, the unsteady drag characteristics of vehicles in a platoon configuration were investigated using URANS and IDDES methods. The results demonstrated that both URANS and IDDES provided significant insights into the aerodynamic interactions and unsteady flow phenomena occurring between Ahmed bodies representing vehicle models. Several key points can be derived.

First, the proper mesh size and calculation settings are essential for determining the computational grid, which affects the results of the unsteady drag coefficient for both the lead and rear vehicle models. Second, the lead vehicle model benefits more from drag reduction compared to the rear vehicle model, as the rear vehicle obstructs the C-pillar vortex, which is the main source of base drag unsteadiness. Third, while URANS shows less unsteadiness in the drag coefficient, the unsteady drag calculated by IDDES shows greater variation because it can capture flow unsteadiness in much more detail. Fourth, the flow field analysis with IDDES reveals a more complex flow phenomenon between the vehicles, causing changes in the drag coefficient of both the lead and rear vehicle models.

Notably, the IDDES approach captured more detailed flow structures and transient effects, leading to a better understanding of unsteady aerodynamic forces. These findings are essential for optimizing platoon configurations to reduce drag and improve fuel efficiency in automotive applications. Nevertheless, improvements can still be made. Future work will aim to (1) further study the IDDES approach for vehicles travelling in platoon configurations, identifying essential factors that affect simulation accuracy, and (2) explore the potential use of machine learning to predict drag behavior in platoon configurations.

ACKNOWLEDGEMENTS

This work is carried out with the funding of the Beasiswa Pendidikan Indonesia (BPI) Puslapdik, together with Lembaga Pengelola Dana Pendidikan (LPDP), with the grant number 3197/BPPT/BPI.LG/IV/2024.

CONFLICT OF INTEREST

The authors declare no conflicts of interest.

AUTHOR CONTRIBUTION

Aan Yudianto: Conceptualization, Methodology, Investigation, Formal Analysis, Data Curation, Writing

REFERENCES

[1] K.. Y. Liang, J. Martensson, and K. H. Johansson, "Heavy-duty vehicle platoon formation for fuel efficiency," *IEEE Transactions on Intelligent Transportation Systems*, vol. 17, no. 4, pp. 1051–1061, 2016.

[2] J. Törnell, S. Sebben, and D. Söderblom, "Influence of inter-vehicle distance on the aerodynamics of a two-truck platoon," *International Journal of Automotive Technology*, vol. 22, no. 3, pp. 747–760, 2021.

[3] H. Dong, J. Shi, W. Zhuang, Z. Li, and Z. Song, "Analyzing the impact of mixed vehicle platoon formations on vehicle energy and traffic efficiencies," *Applied Energy*, vol. 377, p. 124448, 2025.

[4] J. Luo *et al.*, "Review on aerodynamic characteristics and energy recovery of vehicle platoon," *Proceedings of the Institution of Mechanical Engineers, Part D: Journal of Automobile Engineering*, vol. 239, no. 1, pp. 11–38, 2025.

[5] A. Yudianto, H. Sofyan, N. A. Fauzi, and others, "Aerodynamic characteristics of overtaking bus under crosswind: CFD investigation," *CFD Letters*, vol. 14, no. 8, pp. 20–32, 2022.

[6] J. Luo, Y. Tie, K. Mi, Y. Pan, L. Tang, Y. Li, et al., "Aerodynamic optimization of mixed platoon Ahmed body vehicles based on response surface method," *International Journal of Numerical Methods for Heat & Fluid Flow*, vol. 34, no. 1, pp. 309–333, 2024.

[7] A. Yudianto, W. Setiawan, F. Julianto, and U. Aminudin, "Aerodynamic study of vehicles in formation under crosswind," in *AIP Conference Proceedings*, AIP Publishing, 2023, p. 020002.

[8] M. G. Connolly, A. Ivankovic, and M. J. O"Rourke, "Drag reduction technology and devices for road vehicles-A comprehensive review," *Heliyon*, vol. 10, no. 13, p. e33757, 2024.

[9] S. Polek, "Development of a Passive Drag Reduction Modification for the 25° Ahmed Body using Large Eddy Simulation," *UNLV Theses, Dissertations, Professional Papers, and Capstones*, University of Nevada, Las Vegas, 2024.

[10] B. Wang, H. Chen, Z. Huang, and H. Lou, "Large eddy simulation of active flow control for aerodynamic drag reduction in vehicle platooning," *Physics of Fluids*, vol. 37, no. 5, p. 055112, 2025.

[11] G. Zhang, X. Song, X. Hu, J. Wang, T. Yu, P. Guo, et al., "A review on the drag reduction of Ahmed body," *Proceedings of the Institution of Mechanical Engineers, Part D: Journal of Automobile Engineering*, p. 09544070241307072, 2025.

[12] A. Altinisik, O. Yemenici, and H. Umur, "Aerodynamic Analysis of a Passenger Car at Yaw Angle and Two-Vehicle Platoon," *Journal of Fluids Engineering*, vol. 137, no. 12, p. 121107, 2015.

[13] A. Yudianto, I. W. Adiyasa, and A. Yudantoko, "Aerodynamics of bus platooning under crosswind," *Automotive Experiences*, vol. 4, no. 3, pp. 119–130, 2021.

[14] J. Cerutti, G. Cafiero, and G. Iuso, "Aerodynamic drag reduction by means of platooning configurations of light commercial vehicles: A flow field analysis," *International Journal of Heat and Fluid Flow*, vol. 90, p. 108823, 2021.

[15] R. M. Pagliarella, S. Watkins, and A. Tempia, "Aerodynamic performance of vehicles in platoons: the influence of backlight angles," *SAE Technical Paper*, 2007-01–1547, 2007.

[16] S. Watkins and G. Vino, "The effect of vehicle spacing on the aerodynamics of a representative car shape," *Journal of Wind Engineering and Industrial Aerodynamics*, vol. 96, no. 6, pp. 1232–1239, 2008.

[17] A. Yudianto, U. Aminudin, W. Setiawan, and F. Julianto, "Aerodynamic investigation of misaligned four-vehicle platoon," in *AIP Conference Proceedings*, AIP Publishing, 2023, p. 020031.

[18] S. D. Marshall, K. Snape, D. Soper, M. Sterling, and S. Gillmeier, "The aerodynamic performance of a platoon of lorries in close-proximity during an overtaking manoeuvre," *Frontiers in Future Transportation*, vol. 5, p. 1356539, 2024.

[19] J. Luo, M. Li, K. Mi, Z. Liang, X. Chen, L. Ye, et al., "Research on aerodynamic characteristics of vehicle platoon under crosswind conditions based on Ahmed body," *International Journal of Numerical Methods for Heat & Fluid Flow*, vol. 34, no. 7, pp. 2766–2807, 2023.

[20] S. R. Ahmed, G. Ramm, and G. Faltin, "Some salient features of the time-averaged ground vehicle wake," *SAE Technical Paper,* no. 840300, p. 34, 1984.

[21] D. Wang, C. Xia, Q. Jia, and Z. Yang, "Effects of Vehicle Numbers and Vehicle Types on Drag Reduction of Platoons with Different Front-Edge Radius," *SAE Technical Paper*, 2023-01–0951, 2023.

[22] D. Pi, P. Xue, W. Wang, B. Xie, H. Wang, X. Wang, et al., "Automotive platoon energy-saving: A review," *Renewable and Sustainable Energy Reviews*, vol. 179, p. 113268, 2023.

[23] P. Spalart and S. Allmaras, "A one-equation turbulence model for aerodynamic flows," in *30th Aerospace Sciences Meeting and Exhibit*, 1992, p. 439.

[24] M. S. Gritskevich, A. V. Garbaruk, J. Schütze, and F. R. Menter, "Development of DDES and IDDES formulations for the k-ømega shear stress transport model," *Flow, Turbulence and Combustion*, vol. 88, pp. 431–449, 2012.

[25] M. L. Shur, P. R. Spalart, M. K. Strelets, and A. K. Travin, "A hybrid RANS-LES approach with delayed-DES and wall-modelled LES capabilities," *International Journal of Heat and Fluid Flow*, vol. 29, no. 6, pp. 1638–1649, 2008.

[26] I. Kohri, T. Yamanashi, T. Nasu, Y. Hashizume, and D. Katoh, "Study on the transient behaviour of the vortex structure behind Ahmed body," *SAE International Journal of Passenger Cars-Mechanical Systems*, vol. 7, no. 2014-01–0597, pp. 586–602, 2014.

[27] T. Tunay, B. Sahin, and V. Ozbolat, "Effects of rear slant angles on the flow characteristics of Ahmed body," *Experimental Thermal and Fluid Science*, vol. 57, pp. 165–176, 2014.

[28] H. Ebrahim and R. Dominy, "Wake and surface pressure analysis of vehicles in platoon," *Journal of Wind Engineering and Industrial Aerodynamics*, vol. 201, p. 104144, 2020.

[29] P. Schito and F. Braghin, "Numerical and experimental investigation on vehicles in platoon," *SAE International Journal of Commercial Vehicles*, vol. 5, no. 1, pp. 63–71, 2012.

[30] G. Romberg, F. Chianese, and R. Lajoie, "Aerodynamics of race cars in drafting and passing situations," *Racing Chassis and Suspension Design*, vol. 90, p. 267, 2004.

[31] M. Zabat, N. Stabile, S. Farascaroli, and F. Browand, "The aerodynamic performance of platoons: A final report," University of California, Berkeley, California, UCB-ITS-PRR-95-35, 1995.